Three-dimensional filamentation of light in laser plasmas

Andrew J. Schmitt
Laser Plasma Branch,
Plasma Physics Division,
Naval Research Laboratory,
Washington, DC 20375

The first calculations of time-dependent laser-plasma fllamentation in three dimensions are reported. These calculations are done with a three-dimensional laser propagation code based on a previous two-dimensional code [Phys. Fluids **31**, 3079 (1988)]. The effect of incident beam structure, and in particular optical smoothing techniques, on the behavior of filamentation is studied. Both ponderomotive and thermal conduction dominated nonlinearities are considered, and calculations are done simulating both homogeneous non-absorbing plasmas and inhomogeneous laboratory plasmas. Random phase screen (RPS) and induced spatial incoherence (ISI) optical smoothing techniques are investigated and compared to generic unsmoothed laser beams. Qualitative examples are presented and scaling studies are done and compared to a simple theoretical analysis, In typical laser-plasma interactions without optical smoothing, three-dimensional effects lead to greatly increased filament intensities, as expected. Peak filament intensities of order 100-500 times the average intensity are routinely observed (without optical smoothing), as compared to earlier twodimensional calculations where peak intensities were of order 10-50 times average. In spite of this tendency to create stronger filaments, three-dimensional filamentation (when measured on a time-averaged basis) can be suppressed by using ISI smoothing. Under the same conditions, instantaneous IS1 intensities can show considerable enhancement, although much less than the unsmoothed beams. RPS smoothing exhibits less filamentation suppression. Under laser-fusion reactor conditions, calculations indicate that ISI suppression can completely eliminate filamentation.

Report Documentation Page

Form Approved
OMB No. 0704-0188

1. REPORT DATE	2. REPORT TYPE	3. DATES COVERED
1991		**00-00-1991 to 00-00-1991**

4. TITLE AND SUBTITLE	5a. CONTRACT NUMBER
Three-dimensional filamentation of light in laser plasmas	5b. GRANT NUMBER
	5c. PROGRAM ELEMENT NUMBER
6. AUTHOR(S)	5d. PROJECT NUMBER
	5e. TASK NUMBER
	5f. WORK UNIT NUMBER
7. PERFORMING ORGANIZATION NAME(S) AND ADDRESS(ES) **Naval Research Laboratory,Plasma Physics Division,4555 Overlook Avenue SW,Washington,DC,20375**	8. PERFORMING ORGANIZATION REPORT NUMBER
9. SPONSORING/MONITORING AGENCY NAME(S) AND ADDRESS(ES)	10. SPONSOR/MONITOR'S ACRONYM(S)
	11. SPONSOR/MONITOR'S REPORT NUMBER(S)

12. DISTRIBUTION/AVAILABILITY STATEMENT
Approved for public release; distribution unlimited

13. SUPPLEMENTARY NOTES
This article appeared in Physics of Fluids B3, 186 (1991)

14. ABSTRACT

15. SUBJECT TERMS

16. SECURITY CLASSIFICATION OF:			17. LIMITATION OF ABSTRACT	18. NUMBER OF PAGES	19a. NAME OF RESPONSIBLE PERSON
a. REPORT **unclassified**	b. ABSTRACT **unclassified**	c. THIS PAGE **unclassified**	**Same as Report (SAR)**	**29**	

I. INTRODUCTION

The laser filamentation instability is a problem in laser fusion research, as it interferes with classical (linear) absorption of laser light in plasmas. It can be caused by perturbations in either the laser intensity or plasma density. These perturbations reinforce one another: where the density is less than the surrounding area, the resulting index of refraction is seen by the laser as a focusing lens, and the laser light intensity increases there. In the region of higher intensity the ponderomotive force or a higher pressure (from increased absorption) pushes plasma away and decreases the density further, completing the unstable feedback loop. This process can only be stabilized by diffraction (when the filament collapses to a few wavelengths in diameter) and/or by some nonlinear laser-plasma instability (like stimulated Raman or Brillouin scatter) that is induced by the locally higher intensity. The induced instabilities are undesirable effects of filamentation, as they can produce hot electrons that preheat the target interior or reduce light absorption. Filamentation amplifies a wide spectrum of perturbations in both the intensity and plasma density. The amplified wavelengths are typically ~10 λ_0 (laser wavelengths) in size, but can be as large as 100 λ_0 across. The longer wavelength perturbations may seed the dangerous Rayleigh-Taylor instability modes.

Future inertial confinement fusion (ICF) research will increase the target (plasma) size, laser energy, and laser pulse length as systems progress towards reactor-scale conditions. All of these changes increase the tendency towards filamentation and its harmful effects. Fortunately, recent advances in optical smoothing promise some relief. In standard (not optically smoothed) laser systems, incident laser "perturbations" are usually of order 100% and more. It is these substantial laser nonuniformities, not plasma density perturbations, that are primarily responsible for the appearance of filamentation in typical laser-plasma experiments. Thus, cleaning up the uniformity of the laser can substantially reduce or eliminate filamentation effects.

We report here the first calculations of time-dependent laser-plasma filamentation in three dimensions. This extends previous work based on a two-dimensional laser-plasma interaction code published in an earlier paper[1] (hereby referred to as AJS1). Three-dimensional effects are expected

to increase the strength and effects of filamentation. A filament undergoing self-focusing increases in intensity as r_f^{-2} in three dimensions (r_f is the filament radius), as opposed to filaments limited to two dimensions which increase only as r^{-1}. As filamentation is inherently nonlinear, we might reasonably expect the increased intensity to disproportionately increase the severity of the effect. Of particular interest here is the impact that three-dimensional behavior has on filamentation of optically smoothed light. Previous work based on a two-dimensional model shows that optical smoothing can greatly suppress or eliminate filamentation. We wish to address the question of whether it will be as effective when three-dimensional effects are included.

We will show that three-dimensional filamentation can be suppressed by optical smoothing when measured on a time-averaged basis. As was the case in two dimensions, the time-averaged intensity probability distribution can exhibit appreciable increases in the higher energy region, even when optical smoothing suppresses the time-averaged intensity spatial profile. An optically-smoothed beam has an intensity distribution that includes higher energy photons than a perfectly uniform beam, although generally less than an unsmoothed beam. These high-energy photons can drive parametric instabilities that respond on the coherence-time scale (1 psec). Some of the reported ISI effects on parametric instabilities[2] can be explained as a suppression of filamentation, although more than filamentation suppression may be needed to explain some results[3]. We will not directly evaluate here the impact of filamentation on levels of parametric instabilities.

II. FORMALISM

The formalism and notation used here is the same as in AJS1, with the addition of the second transverse spatial dimension. The Maxwell wave equation governing the propagation of the laser light is simplified by transforming out the high-frequency space and time variations, along with background absorption and field swelling effects. The resulting parabolic wave equation describes the evolution of the wave envelope, Ψ, which is assumed to be slowly varying compared to the high-frequency variations:

$$\left(4\pi i \frac{\partial}{\partial \eta} - \nabla_\perp^2\right)\psi = 4\pi^2 \delta\varepsilon\ (\eta, x, y, t)\ \psi \qquad (1)$$

The transverse Laplacian is now $\nabla_\perp^2=\nabla_x^2+\nabla_y^2$, and the axial coordinate is $\eta = \int^z dz'\omega_o/ck_o(z)$. As in AJS1, the subscript "o" here and elsewhere refers to evaluation of the quantity at the background value, and an overbar "−" refers to normalization of a quantity to its value at the background. $\delta\varepsilon = \varepsilon(\eta,x,y,t)-\varepsilon_o(\eta)$, the change in the dielectric constant from its average value, is responsible for filamentation and other effects due to the em wave interaction with the plasma. In this model, $\delta\varepsilon$ is determined by the local density of the plasma.

The plasma dynamics are treated by assuming a plasma which is allowed to move in the transverse direction, but is (quasi-)stationary in the axial direction. Neglect of axial flow is generally reasonable[4], and neglect of a changing plasma background is reasonable if the filamentation time is much smaller than the time-scale for the background to change[5]. The plasma motion is described by a quasi-linearized, damped ion-acoustic wave equation driven by temperature gradients and the ponderomotive force:

$$\left(\frac{\partial^2}{\partial t^2} + \frac{\nu\lambda_0}{C_s}\frac{\partial}{\partial t} - \nabla_\perp^2\right)\ln(\bar{n}_e) = \frac{1}{(1+1/Z)}\nabla_\perp^2\bar{T} + \gamma_p\nabla_\perp^2\bar{I} \qquad (2)$$

The usual value of the damping coefficient q ($q=\nu/C_s$) is taken to be 1/2, corresponding to a plasma where the electron and ion temperatures are comparable. The temperature distribution is determined by a time-dependent balance between electron thermal conduction and inverse bremsstrahlung heating:

$$2\pi\gamma_R\bar{n}_e\frac{\partial}{\partial t}\bar{T} = \vec{\nabla}_\perp\cdot\bar{\kappa}_e\vec{\nabla}_\perp\bar{T} + 4\pi^2\gamma_T\bar{I} \qquad (3)$$

The nondimensional terms in the above equations are:

$$\gamma_p = \frac{e^2\psi_o^*\cdot\psi_o}{4m_e\omega_o^2T_{eo}(1+1/Z)} \equiv \frac{\text{ponderomotive pressure}}{\text{plasma thermal pressure}} \qquad (4a)$$

$$\gamma_R = \frac{3}{2}\frac{C_{so}n_{eo}c}{\kappa_{eo}\omega_o} \equiv \frac{\text{thermal conduction transit time across } k_o^{-1}}{\text{ion-acoustic transit time across } k_o^{-1}} \qquad (4b)$$

$$\gamma_T = \frac{c^2\kappa_bI_o}{\omega_o^2\kappa_{eo}T_{eo}} \equiv \frac{\text{inverse bremsstrahlung heating rate}}{\text{thermal conduction cooling rate across } k_o^{-1}} \qquad (4c)$$

Two key nondimensional parameters characterize the strength of the filamentation interaction: γ_p, the ratio of electric field pressure to the plasma thermal pressure, and γ_T, the ratio of the inverse bremsstrahlung heating rate to the thermal conduction loss rate at wavelength-size scale lengths. These parameters give the magnitude of ponderomotive and thermal filamentation, the two different filamentation mechanisms that are analyzed separately here. The ponderomotive force, proportional to λ_0^2 (the square of the laser wavelength), usually dominates for longer laser wavelength plasma interactions ($\lambda_0 \geq 0.5\ \mu$m), while thermal filamentation, proportional to T_e^5, is important for cooler plasmas that are more common with shorter wavelength lasers.

In contrast to the earlier two-dimensional studies, no flux-limiting is applied to the electron thermal conduction. Generally, simulations were done under conditions where flux-limiting was not warranted. Moreover, recent results on thermal conduction in laser-plasmas show that the simple flux-limiting model may be too simplistic[6]; in any event the subject will not be treated here.

As discussed in the previous paper, a time-independent version of these equations is used in problems that have a quasi-steady-state input intensity. This assumes that the sound transit time across the plasma or beam is much smaller than the laser pulse width. In addition, if the plasma propagation length is very long, there are certain conditions under which equilibrium can be delayed[7]; however, these considerations are beyond the scope of the present analysis.

III. Analysis and Discussion

Three types of beams are studied here, and are described briefly in the next section. Following this, we will examine how the different beam structures affect the filamentation instability.

A. Beam types

The first type of beam, which we label generic, represents non-optically smoothed systems (as an example, see Fig. 1a). Although most common, the intensity distributions of these beams as a whole are the least well known, partly because they are quite sensitive to the details of the optical design and system. However, they are distinguished as having little bandwidth (and thus stationary illumination patterns) and a great deal of intensity structure (peak intensities are often many times

the average intensity). We model them here (as in AJS1) by assuming that the laser electric field has a uniform distribution in Fourier space (in the plane transverse to propagation), except for the DC term. The Fourier spectra is limited in extent by the spot size and f-number of the lens. A free parameter that is varied is the standard deviation of the intensity distribution, defined as $\sigma_{rms} = (\int(I-I_{avg})^2/I_{avg}^{2)1/2}$. The standard deviation is used here as a measure of the quality of the generic beam. It is varied in the code by adjusting the ratio of the AC terms to DC term in the Fourier spectra.

The second beam type is generated by the simplest optical smoothing method: random phase smoothing (RPS)[8]. This scheme requires no laser bandwidth, so it can be relatively easy to implement on existing laser systems. A random phase screen, composed of many areas that shift the laser phase by either 0 or π, is placed in the optical beam path. These small phase-shifting areas each produce a higher quality beamlet that is in phase with only half the others. The resulting focused distribution looks very chaotic (Fig. 1b), but it has a controllable envelope profile determined by the shape of the phase-shifting areas on the screen. If enough high frequency spatial structure can be generated in the profile (by using fast lenses) the distribution will theoretically resist filamentation.

The third beam type described here is produced by the induced spatial incoherence (ISI) method[9,10]. Conceptually, this consists of a beam mask similar to the one used in the RPS method. In addition, each phase-shifting area is designed to produce a beamlet that is incoherent relative to all the other areas. This requires bandwidth on the laser beam. The beam profile in this case looks similar to the RPS method at any instant, but changes on the time scale of the laser coherence time, usually about a picosecond or so. On time scales much longer than this, the intensity structure is randomly time-averaged to a smooth profile (Fig. 1c), determined again by the geometric shape of the phase shifting area. The recently developed echelon-free ISI technique[10] gives the same intensity behavior at the target while allowing much more flexibility in the beam envelope shape.

Although not separately addressed here, the recently developed smoothing by spectral dispersion technique[11] (SSD) should behave in a manner similar to ISI. Although it is not strictly

speaking incoherent, it relies upon bandwidth and spatial incoherence to produce smoothing. Some differences are that SSD preferentially smooths in one direction, leaving more residual structure in the other transverse dimension. Also, SSD smooths by sweeping Fourier components of the distribution in a linear motion; some of these components may be resonant with the plasma sound speed and experience enhanced filamentation tendencies[4,12].

The numerical construction of these beams in the code is done in the same manner as described in AJS1, with straightforward extensions to include the second transverse dimension.

B. Qualitative filamentation behavior

As an example of a simulation of laser-plasma interaction experiments, the results of green laser light (frequency-doubled glass laser light at 0.53 μm) interacting with a plastic (CH) plasma are shown in Fig. 2. The parameters shown are typical of current ICF research experiments (they come from hydrocode simulations of NRL experimental studies with the Pharos III laser[3]); the incoming beam has peak-to-average intensity variations of about 8-to-1, and a root-mean-square deviation of σ_{rms}=1. The initial intensity profile is constructed as discussed in section III.A. The pictures at the bottom of the figure show images of the laser profile at different planes as it propagates into the plasma. These images are designed to emulate film negatives: the darker areas are areas of higher intensity, and the image density is proportional to the logarithm of the light intensity. The calculation assumes steady state conditions, which should be appropriate for the long pulse (few nsecs), narrow-bandwidth interactions being simulated.

This sequence of images shows the intense spots in the light distribution focusing down into filaments. After forming, they often diffract a significant proportion of the light outward in the diffraction rings seen in the latter images, like raindrops rippling the surface of a pond. The filaments start to form where the background density is ~0.13 times critical, and have characteristic peak intensities of several hundred times average. The highest intensity reached in this simulation was over 1.5×10^{17} W/cm^2, or more than 600 times the average intensity.

This particular example is dominated by ponderomotive filamentation. A characteristic of this type of filamentation is that the filaments act independently, with very little influence on the

propagation of other filaments. What little interaction there is often occurs in the diffraction rings thrown off by a filament Usually, these rings are of low enough intensity (and fairly one-dimensional) that they do not produce filaments themselves, but occasionally interference between two or more rings from close filaments can produce another filament.

In contrast, filaments produced by thermal filamentation tend to attract one another into large clusters. Fig. 3 illustrates an example of thermal filamentation of a 0.25μm wavelength laser at 4×10^{14} W/cm^2 in an ideal homogeneous plasma with a background density of 0.5 n_{crit} and electron temperature 1 keV, giving an coupling strength of $\gamma_T=2.1\times10^{-6}$, which is a typical value. Although the laser is allowed to create the needed temperature gradients for thermal filamentation to occur, no light absorption (pump depletion) is allowed. The simulation shows that thermally-driven filaments form and collect light over a much broader area than the ponderomotive filaments, attracting other filaments in the process. The end result is a single large cluster of many filaments, limited in size only by the simulation dimensions. This clustering behavior is due to the large density cavities that are created by long temperature gradients, as explained in AJS1.

C. Quantitative filamentation behavior

Quantitative studies of thermal and ponderomotive filamentation in homogeneous, non-absorbing plasmas show the scaling of the focal distance and intensity maxima as a function of the coupling strength parameters γ_p and γ_T. The results, shown in Fig. 4, are compared to the predictions of the simple theoretical analysis presented in AJS1. Several different methods are used to measure the filamentation parameters shown in Fig. 4 and the succeeding figures. First, the maximum intensity as a function of the propagation distance is found by searching the intensity distributions in x and y at a given z. Then, maxima of this function (e.g., Fig. 3 or the inset in Fig. 2) are used to quantify filamentation. The intensity maxima are measured and classified as either the first intensity maximum that is exhibited along the propagation direction of the laser beam, or the absolute largest intensity maximum. The former indicates the occurrence of first focus (and can be compared to the simple theory), while the latter quantifies the severity of the filamentation. The absolute intensity maximum is somewhat dependent upon the axial extent of the plasma simulated:

there is always some chance that an even larger intensity maximum awaits us further in the distance. (In practice, filamentation behavior usually saturates within a certain distance; further propagation results in fluctuations on a gently decreasing background. In the real world, absorption and other dissipative processes will also eventually stop filamentation.) Another method of defining the filamentation parameters is to use the distance and value at which the 90%-energy intensity is maximum. 90% of the total beam energy is found at intensities below the 90%-energy intensity, and 10% of the total beam energy is above it. This measurement more accurately expresses the behavior of the entire intensity distribution, as opposed to the intensity maximum which indicates the maximum extent of the distribution.

The effectiveness of the RPS optical smoothing technique is analyzed with a series of simulations of laser propagation into homogeneous plasmas. The ponderomotive and thermal filamentation mechanisms are studied separately by arbitrarily setting one term or another to zero in the governing equations, and pump depletion is again neglected. These simulations are done with 0.25 μm light at 8×10^{14} W/cm^2, a background temperature of 1 keV, and a background density of 0.5 n_{crit}, giving coupling parameters of $\gamma_p = 5\times10^{-3}$ and $\gamma_T = 2\times10^{-6}$. Additionally, the incident laser beams have an rms deviation of 0.5. (In true RPS, the rms deviation is greater than one. However, this difference should not affect the scaling. The magnitude of the filamentation may be slightly weaker here, but this only reinforces the conclusions.) The f/number of the lens was then varied to determine its effect on filamentation. We expect that as the lens becomes faster (i.e., the f/number decreases), less filamentation would be observed. The results, presented in Fig. 5, bear out the expectation. However, even the smallest f/numbers (f/2.5) were unable to completely resist filamentation. In addition, the requirement for fast lenses for this method is contrary to the need for large f/number optics in laser fusion systems. (Larger f/number lenses will be needed in part to minimize the total optical area exposed to the effects of an ICF implosion.) Generally, RPS is not a satisfactory method for reducing filamentation effects.

ISI is also analyzed using a series of simulations in which the strength of the coupling terms (γ_p and γ_T) and the coherence time are independently varied. $\gamma_p\tau_c^{1/2}$ and $\gamma_T\tau_c^{1/2}$ are expected to be

the relevant scaling factor for the ISI coupling strength[1] (τ_c is the coherence time, t_c, divided by λ_0/C_s). This can be heuristically explained by noting that the net force felt by the plasma depends on the instantaneous magnitude of the force ($\propto \gamma_p$ or γ_T) averaged over a number of (random) realizations (giving the contribution $\{t_c/t_{avg}\}^{1/2}$). The relevant averaging time is assumed to be dependent on the wavenumber (spatial width) of the potential filament, $t_{avg} \sim (k_\perp C_s)^{-1}$. As discussed in the earlier paper, two types of intensity maxima are measured; the first is the time-averaged maximum intensities, the second type is the maximum time-averaged intensities. Time averages are typically performed over 100 t_c. The first type of intensity maximum represents typical values that may be sensed by quickly-acting plasma processes (quick compared to the laser coherence time, t_c; laser-plasma instabilities such as SRS or SBS may be in this category), whereas the latter are the intensity maxima that are felt by time-averaging (i.e., larger-scale hydrodynamic) processes.

Fig. 6 (ponderomotive only) and Fig. 7 (thermal only) illustrate typical examples of these ISI simulations. Parameters for these simulations are $\gamma_p = 1\times10^{-2}$, $\tau_c = 1$ for the ponderomotive case and $\gamma_T = 1.98\times10^{-6}$, $\tau_c = 0.54$ for the thermal case. The initial intensity profiles are constructed as discussed in section III.A for ISI beams. In each figure, a sample instantaneous intensity profile at succeeding axial points in the plasma is shown (as in Fig. 2); these profiles persist over a laser coherence time or less. For comparison, each figure also shows the intensity profiles at the same axial positions, time-averaged over 100 laser coherence times. The instantaneous intensity profiles exhibit the same patterns as shown earlier in simulation of the generic beam filamentation (Fig. 2 & Fig. 3). The key differences are that the peak intensities are not as large, the intensity profiles are constantly changing, and the time-averaged intensities are much smoother, although some time-averaged structure can persist.

Scaling of the filamentation parameters with ISI smoothing is shown in Fig. 8, plotted as a function of the coupling terms, $\gamma_p\tau_c^{1/2}$ and $\gamma_T\tau_c^{1/2}$. The theoretical focal length scalings (from Table II in paper AJS1) are consistent with the thermal data (although there is a fair amount of scatter), while the ponderomotive data shows a scaling that is more complex than a simple power

law in $\gamma_p\tau_c^{1/2}$. (The apparent persistence of ponderomotive filamentation at low values of $\gamma_p\tau_c^{1/2}$ is most likely the transition to a regime where random propagation and scattering of the light becomes dominant over filamentation. The intensity maxima shown reinforce this, since they are about what would be expected for linear propagation of the light) The plots of intensity vs. coupling strength show two clusters of data points. Measurements of the time-averaged intensity distribution tend to show intensity maxima smaller than 10 times average, while the time-averaged measurements of instantaneous peak intensities show intensities approaching 100 times average. It appears that the filamentation mechanisms can produce short-term intensity enhancement, but these enhancements are smoothed out during the time averages.

To examine in more detail how ISI smooths the laser beam, we can look at the laser energy distribution as the light propagates into the plasma. It is worthwhile to understand how this energy distribution is modified by filamentation forces, so that we might estimate (for instance) how much energy is available to drive a certain instability with a given threshold intensity. As an example, Fig. 9 shows the integrated energy distribution for both ISI and non-smoothed beams before and after propagation to 0.5 n_{crit} in the 1/2 μm laser-plasma interaction shown in Fig. 2. The actual plotted data is the fractional energy of the intensity distribution that occurs at intensities less than a given intensity, I/I_0 where I_0 is the time-averaged laser intensity. This is found by integrating the intensity distribution over a transverse plane at a given point during propagation:

$$\text{Integrated Energy}(I/I_0,z) = \int_0^{I/I_0} \tilde{I}/I_0 \; P(\tilde{I}/I_0,z)\, d\,\tilde{I}/I_0 \qquad (5)$$

where $P(I/I_0, z)$ is the intensity distribution at the plane z. For the incident ISI beam, the intensity distribution is given by $P(I/I_0,z=0) = \exp(-I/I_0)$, and the integrated energy is $1-(1+I/I_0)\exp(-I/I_0)$. The plot on the left-hand-side of Fig. 9 shows that the incident ISI beam has an intensity distribution that is equivalent to a generic beam with a root-mean-square deviation of about 1. However, when compared to that same beam after both have propagated to 0.5 n_{crit}, the plot on the right shows that the ISI beam distribution has not changed very much (the maximum instantaneous

intensity is about 20 times average), while the unsmoothed beam has approximately 25% of its energy at intensities greater than 20 times the average (and a maximum intensity about 600 times average).

We have seen that the magnitude of the ISI smoothing effect can depend somewhat on the particular details of the experiment - the laser intensity, density scale length (i.e., propagation distance), etc. A practical question, though, is whether or not ISI will provide enough filamentation suppression to be useful in large-scale, reactor-size ICF targets. The brief answer is that ISI appears to be able to completely eliminate filamentation in such targets at short laser wavelength (0.25 μm).

Fig. 10 illustrates a simulation of ISI smoothing on a DT pellet irradiated by 5 MJ of KrF laser light at 3×10^{14} W/cm^2. The pellet dynamics are first calculated by the FAST1D hydrocode[13], and then the plasma density and temperature profiles are postprocessed with the laser propagation code to calculate the filamentation. The density and temperature profiles were shown in AJS1, fig. 22c, where the analogous 2-D simulation was done. Both ponderomotive and thermal filamentation mechanisms are included in this simulation. A sample "snapshot" of the intensity distribution and a $100t_c$ time-averaged intensity distribution are shown at different background densities in the plasma. Neither of these distributions shows any evidence of filamentation. By comparison, steady state simulations of unsmoothed beams in this particular plasma indicate that the rms standard deviation must be less than 0.65 to control filamentation effects. A simulation of a laser beam incident on this plasma with σ_{rms}=0.65 produces a filament with a peak intensity greater than 300 times average.

In another, more challenging example with a longer scalelength and higher ionization, the conclusions are similar. A FAST1D simulation is performed of a reactor target coated with a CH ablator and illuminated with a 3.6 MJ KrF pulse, with nominal peak intensity of 3.5×10^{14} W/cm^2. The resulting plasma is quite large (about 2.6×10^4 laser wavelengths, or 700 μm, between 0.01 and 0.75 n_{crit}) with temperatures ranging from 1.5 keV at .01 n_{crit} to a maximum of 3.1 keV near 0.3 n_{crit}. An ISI beam with t_c = 1 psec and various quality generic beams are propagated through

this plasma to show the gains achievable by optical smoothing. As can be seen (Fig. 11) by a comparison of the maximum intensities as a function of the propagation distance in the plasma, the ISI beam (both instantaneous and time-averaged intensity maxima) remains almost unchanged while all cases of the generic beam undergo filamentation, even for σ_{rms} as low as 10%. Improving the optical quality without smoothing in this case merely delays the start of filamentation to higher densities. Optical smoothing must be used to avoid filamentation.

IV. CONCLUSIONS

As expected, calculations of three-dimensional filamentation show much stronger filamentation behavior than previous two-dimensional studies. In generic laser beams that are not optically smoothed and susceptible to filamentation, intensity increases tend to produce filaments with peak intensities that are a hundreds of times the average laser intensity. Imposing only spatial incoherence on the beams (i.e., using random phase screens) results in minor reductions of filamentation effects at the expense of being forced to use fast focusing optics. Optical smoothing by methods that produce temporal and spatial incoherence in the laser (such as ISI) produce a qualitatively different, and more complex, behavior. In general this type of smoothing reduces the severity of the filamentation effect, and can eliminate it altogether in some cases. However, if the filamentation mechanism is strong enough, the intensity distribution of an optically smoothed beam may still produce peak intensities that are 50-100 times the average intensity. This phenomena is most important to instabilities that can react on a fast time scale, on the order of the laser coherence time (this generally includes the undesirable parametric scattering instabilities). On the other hand, even when this instantaneous intensity enhancement occurs, the time averages of the intensity distribution reveal that these filamentary patterns are not stationary, and the time-averaged intensity enhancements are only of order a few times average.

Optical smoothing by ISI is generally more effective in laboratory plasmas than in the ideal homogeneous nonabsorbing plasmas used in some of these simulations. In laboratory plasmas, filamentation is further constrained by plasma inhomogeneity (which limits the allowed filamentation growth length) or by absorption. Since ISI can delay the onset of filamentation as

well as suppress the effects, these constraints can cause ISI to eliminate filamentation entirely in these plasmas.

Finally, we note that the common theoretical approximation of a uniform or single laser intensity is not warranted. Generally, the laser light has a distribution of intensities that can be severely altered by filamentation. Most theoretical treatments of nonlinear light-plasma interaction to date have ignored this effect. One side benefit of optical smoothing is that this intensity distribution is generally easier to control and understand than the generic filamentation-dominated light distribution.

ACKNOWLEDGEMENTS

The author would like to acknowledge valuable discussions with Dr. S. Bodner, Dr. R. Lehmberg, and Dr. S. Obenschain. This research was supported by the U.S. Department of Energy. Software from the National Center for Supercomputing Applications (NCSA Telnet and NCSA Image) has also been helpful in the development and analysis of this work.

REFERENCES

1. A.J. Schmitt, Phys. Fluids **31**, 3079 (1988).
2. S.P. Obenschain, J. Grun, M.J. Herbst, K.J. Kearney, C.K. Manka, E.A. McLean, A.N. Mostovych, J.A. Stamper, R.R. Whitlock, S.E. Bodner, J.H. Gardner, and R.H. Lehmberg, Phys. Rev. Lett. **56**, 2807 (1986); S.P. Obenschain, C.J. Pawley, A.N. Mostovych, J.A. Stamper, J.H. Gardner, A.J. Schmitt, and S.E. Bodner, Phys. Rev. Lett. **62**, 768 (1989); S.E.Coe, T. Afshar-rad, M. Desselberger, F. Khattak, O. Willi, A. Giulietti, Z.Q. Lin, W. Yu, and C. Danson, Europhys. Lett. **10**, 31 (1989).
3. A.N. Mostovych, S.P. Obenschain, J.H. Gardner, J. Grun, K.J. Kearney, C.K. Manka, E.A. McLean, and C.J. Pawley, Phys. Rev. Lett. **59**, 1193 (1987); T. Peyser, private communication.
4. R.W. Short, R. Bingham, and E.A. Williams, Phys. Fluids **25**, 2302 (1982); F. Cornolti and M. Lucchesi, Plasma Physics and Controlled Fusion **31**, 213 (1989); A.J. Schmitt, Phys. Fluids **B1**, 1287 (1989).
5. M.S. Sodha, J.K. Sharma, R.P. Sharma, and S.C. Kaushik, J. Appl. Phys. **49**, 599 (1978); A.J. Schmitt and R.S.B. Ong, J. Appl. Phys. **54**, 3003 (1983).
6. E. Epperlein, G.J. Rickard and A.R. Bell, Phys. Rev. Lett. **61**, 2453 (1988).
7. S. Coggeshall, W.C. Mead, and R.D. Jones, Phys. Fluids **31**, 2750 (1988); J. Limpouch, G. Loncar, I.G. Lebo, and V.B. Rozanov, Laser and Particle Beams **6**, 295 (1988); H.A. Rose, D. Russell, and D.F. DuBois, Bull. Am. Phys. Soc. **34**, 1938 (1989).
8. Y. Kato and K. Mima, Appl. Phys. **B29**, 186 (1982).
9. R.H. Lehmberg and S.P. Obenschain, Opt. Commun. **46**, 27 (1983).
10. R.H. Lehmberg and J. Goldhar, Fusion Technol. **11**, 532 (1987); R.H. Lehmberg, A.J. Schmitt, and S.E. Bodner, J. Appl. Phys. **62**, 2680 (1987).
11. S. Skupsky, R.W. Short, T. Kessler, R.S. Craxton, S. Letzring, and J.M. Soures, J. Appl. Phys **66**, 3456 (1989).
12. R.W. Short, Bull. Am. Phys. Soc. **34**, 2113 (1989).
13. J.H. Gardner and S.E. Bodner, Phys. Fluids **29**, 2672 (1986).

FIGURE CAPTIONS

Fig. 1. The three types of beams studied here are (a) generic, representing a typical beam without optical smoothing; (b) a beam that has been smoothed using RPS; and (c) an ISI smoothed beam. All profiles shown are time averages over the entire pulse. At top are shown the beam intensity profiles on target, and below are representative line-outs of the intensity.

Fig. 2. Example of filamentation in an inhomogeneous CH plasma with an approximate density scale length of 150 μm. The plasma is created by a 100J green (λ_0=0.53 μm) laser pulse at 2×10^{14} W/cm^2, with initial peak-to-average intensity fluctuations of 8.5:1 (σ_{rms}=1.0). The steady state filamentation model is used here to calculate the laser propagation. The pictures at the bottom here (and in others figures in this paper) show the intensity profile at planes successively deeper into the plasma (denoted by the arrows). The dark areas of the pictures are regions of higher intensity, and their density is proportional to the logarithm of the intensity, as in film negatives. This filamentation is dominated by the ponderomotive mechanism, although thermal filamentation is also included in the calculation. The inset plot shows the maximum intensity vs. propagation distance, z.

Fig. 3. An example of thermal filamentation in a homogeneous, nonabsorbing plasma. $\gamma_T = 2.1\times10^{-6}$. These intensity profiles are taken during the propagation at intervals of 250 λ_0. The steady state filamentation model is used here to calculate the laser propagation.

Fig. 4. The scaling of focal length and maximum intensity is shown for generic beams in homogeneous, nonabsorbing plasmas. The theoretical scalings are taken from from Table I in paper AJS1.

Fig. 5. In simulations of the RPS method, filamentation is reduced but still appreciable when the *f*/# of the focusing optics is decreased. The open symbols in these figures denote ponderomotive filamentation only, while the filled symbols correspond to thermal filamentation only. In addition, there are two symbols for each filamentation mechanism:

the square denotes the intensity or growth distance at which the first filament focus occurs, while the cross denotes point at which the most intense filament is found. All simulations were done with the following parameters: 0.25 μm wavelength laser, average intensity 8×10^{14} W/cm^2, background electron temperature 1 keV, and background electron density 0.5 n_{crit}. The coupling strengths are $\gamma_p = 5\times10^{-3}$ and $\gamma_T = 2\times10^{-6}$.

Fig. 6. Results of simulations with ISI: an example of ponderomotive filamentation in a non-absorbing, homogeneous plasma. The intensity profiles are shown in the fashion of Fig. 2, with propagation occurring from left to right; the top row shows typical instantaneous intensity profiles, and the bottom row shows time-averaged profiles over $100\tau_c$. Profiles are shown at propagation distance intervals of 333 λ_0. Parameters for the simulations are $\gamma_p = 1\times10^{-2}$, $\tau_c = 1$ with f/10 focusing optics.

Fig. 7. Results of simulations with ISI: an example of thermal filamentation in a non-absorbing, homogeneous plasma. The profiles are shown as in Fig. 6 with instantaneous profiles on top, the time averages on the bottom, and the profiles are shown at intervals of 167 λ_0. Parameters for the simulations are $\gamma_T = 1.98\times10^{-6}$, $\tau_c = 0.54$ with *f*/20 focusing optics.

Fig. 8. Results of simulations with ISI: variation of focal lengths and intensity maxima as a function of nondimensional coupling strength for (a) ponderomotive and (b) thermal mechanisms. The theoretical scalings are taken from from Table II in paper AJS1.

Fig. 9. A comparison of the integrated energy distributions of laser light for both ISI and non-smoothed optical laser beams: (a) shows the energy distribution at the beginning of the plasma, (b) shows the distribution after the beams have propagated to .5 n_e/n_{crit}. Both beams are enhanced in the high energy region, but the non-smoothed beam is especially altered. Plasma parameters are the same as for Fig. 2.

Fig. 10. Results of simulations with ISI: smoothing on DT-pellet plasma created by 5 MJ of KrF light at 3×10^{14} W/cm^2. Instantaneous profiles are shown at top, time-averaged profiles are shown at bottom. The laser has a coherence time of 0.9 psec.

Fig. 11. Comparison of ISI-smoothed and generic beams on a CH reactor pellet ablator created by 3.6 MJ of KrF light at 3.5×10^{14} W/cm^2: maximum intensities are shown as the beam propagates into the plasma. Both the time-averaged maximum intensity and the maximum time-averaged intensity are shown for the ISI beam (t_c=1.03 psec). The bottom axes show both the propagation distance and background electron plasma density in the plasma.

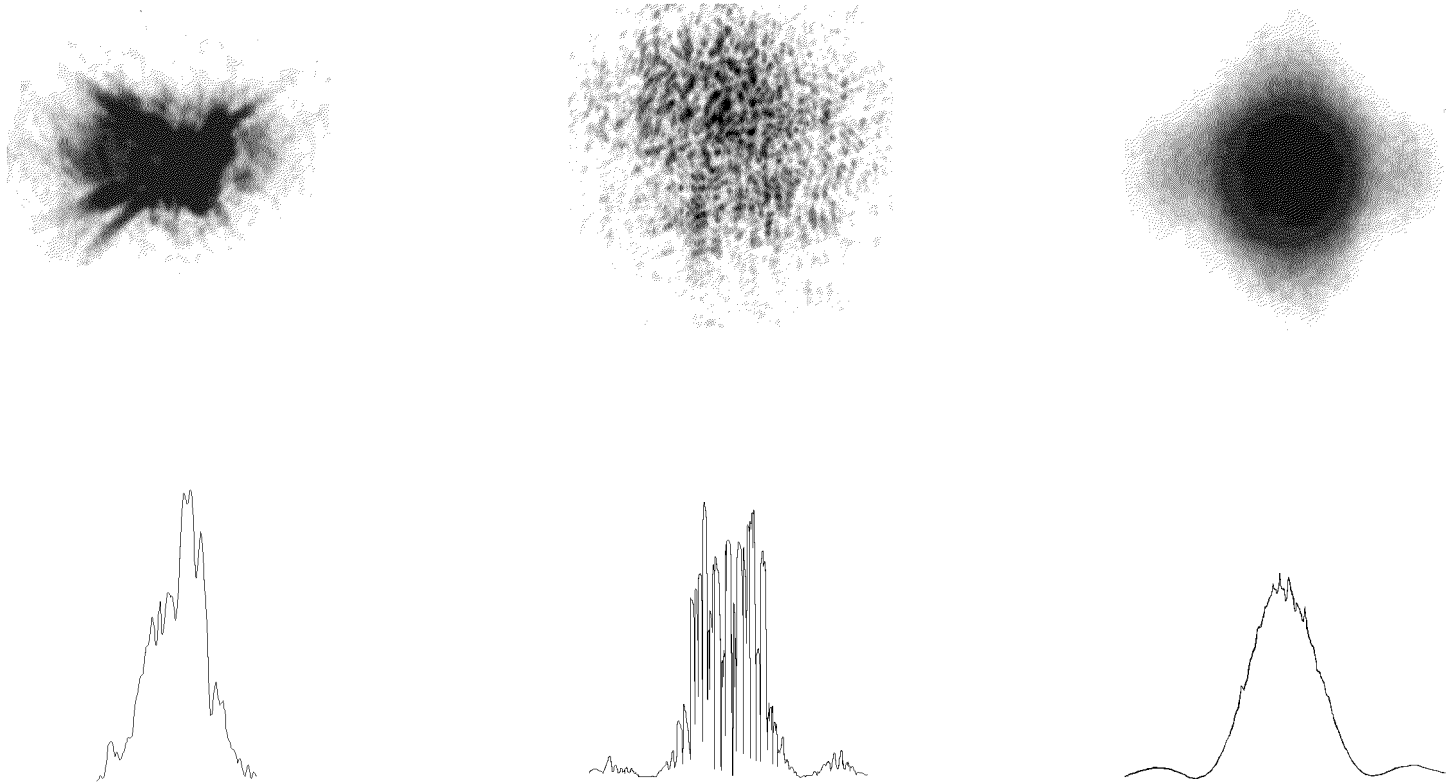

(a) generic beam (b) RPS beam (c) ISI beam

Fig. 1

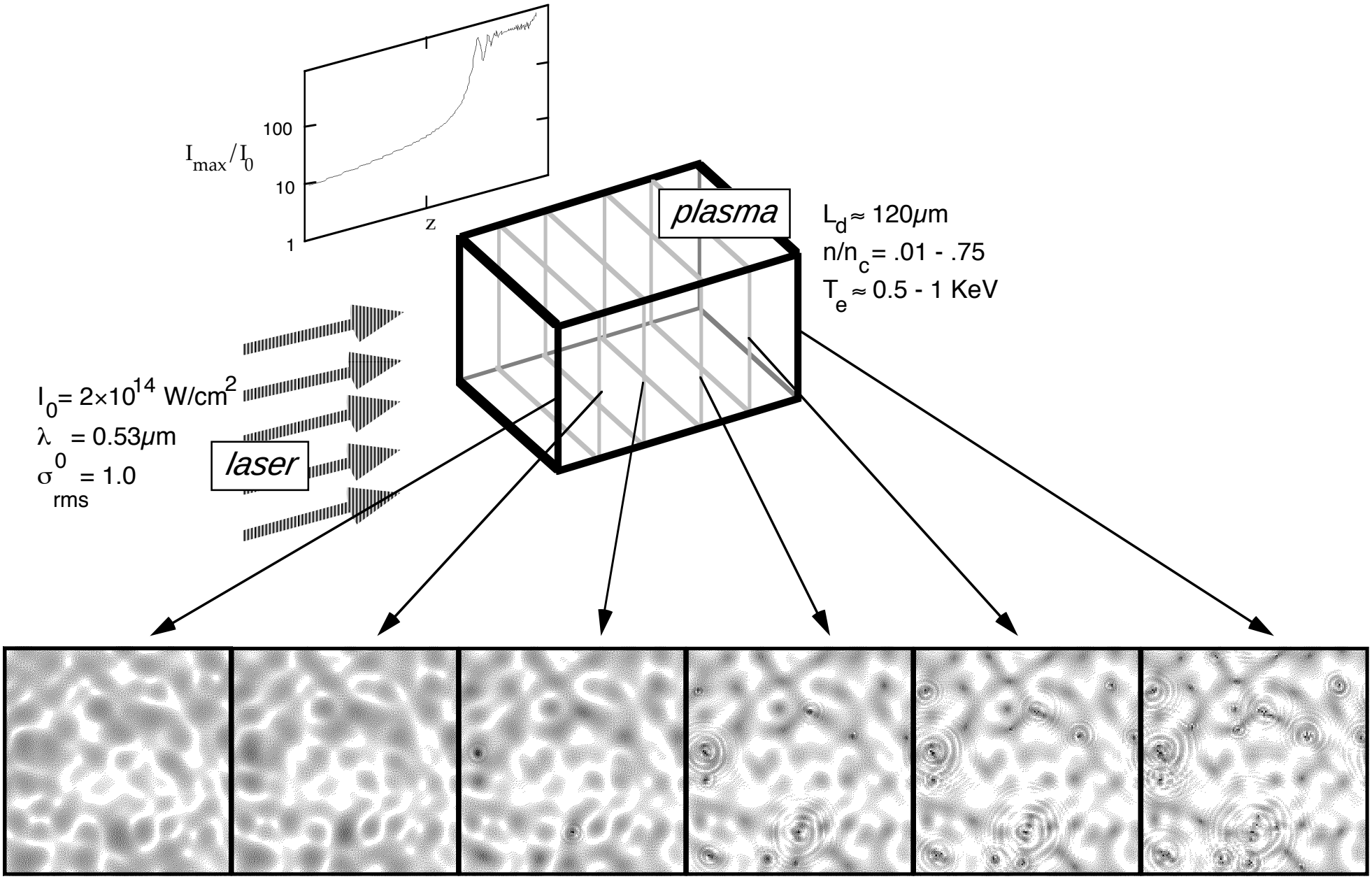
I_{max}/I_0
100
10
1
z
plasma
$L_d \approx 120\mu m$
$n/n_c = .01 - .75$
$T_e \approx 0.5 - 1$ KeV
$I_0 = 2\times10^{14}$ W/cm^2
$\lambda = 0.53\mu m$
$\sigma^0_{rms} = 1.0$
laser

Fig. 2

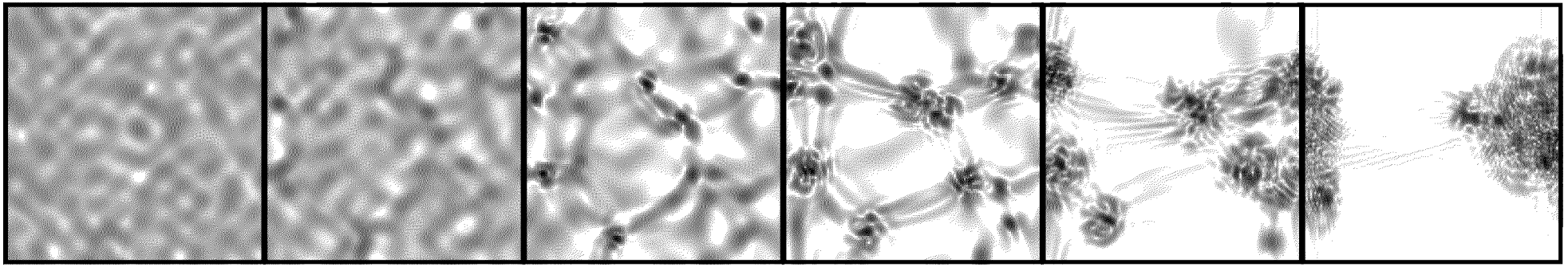

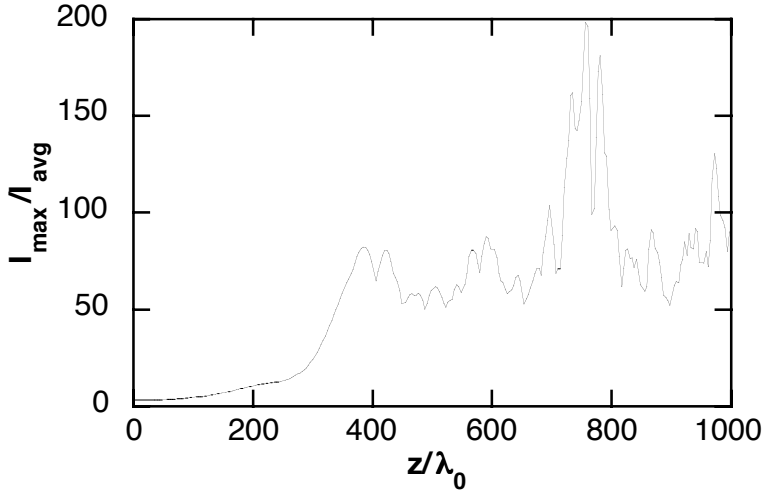

Fig. 3

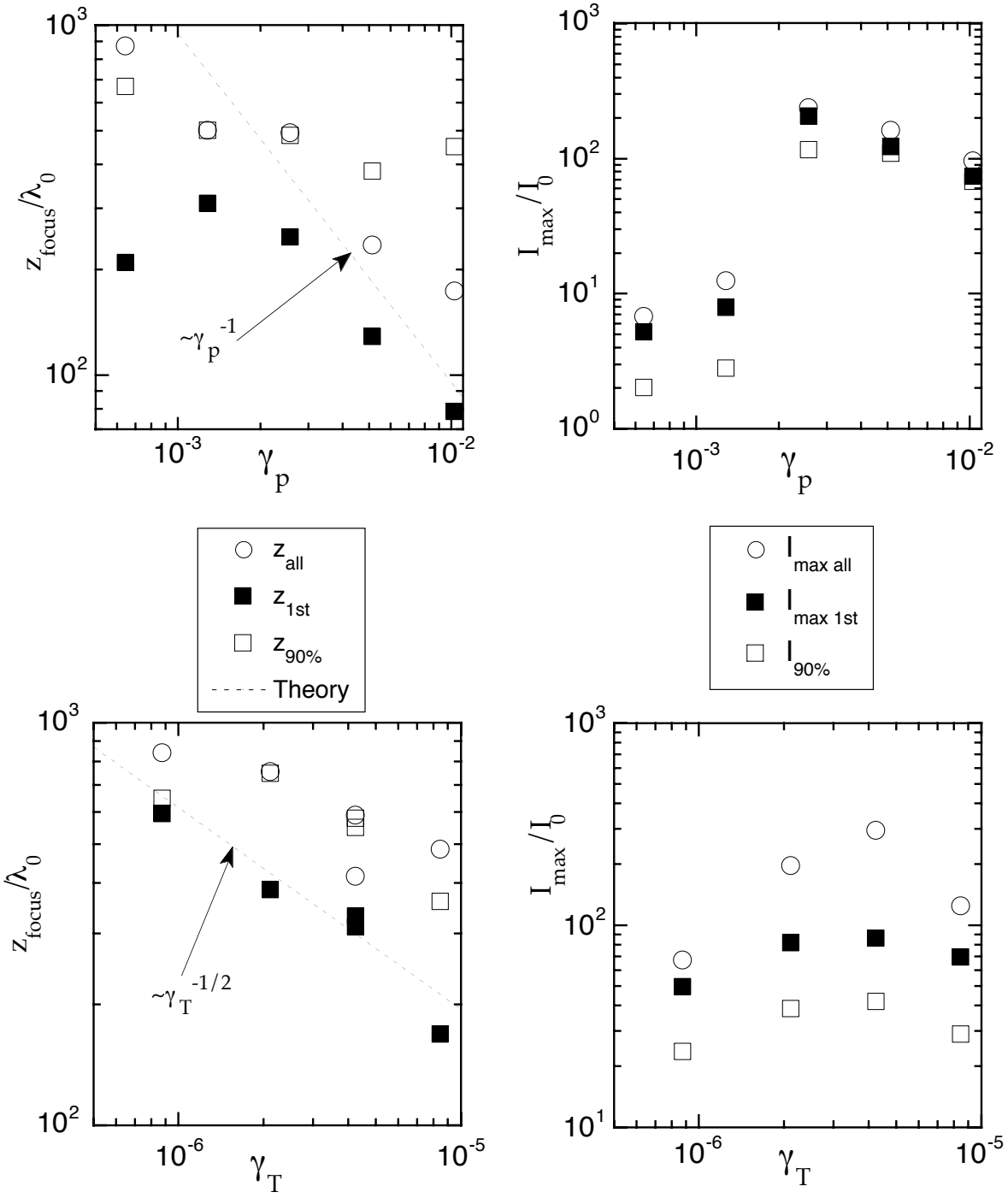
10^3
10^2
z_{focus}/λ_0
$\sim\gamma_p^{-1}$
10^{-3}
γ_p
10^{-2}
10^3
10^2
10^1
10^0
I_{max}/I_0
10^{-3}
γ_p
10^{-2}
z_{all}
z_{1st}
$z_{90\%}$
Theory
$I_{max\ all}$
$I_{max\ 1st}$
$I_{90\%}$
10^3
10^2
z_{focus}/λ_0
$\sim\gamma_T^{-1/2}$
10^{-6}
γ_T
10^{-5}
10^3
10^2
10^1
I_{max}/I_0
10^{-6}
γ_T
10^{-5}

Fig. 4

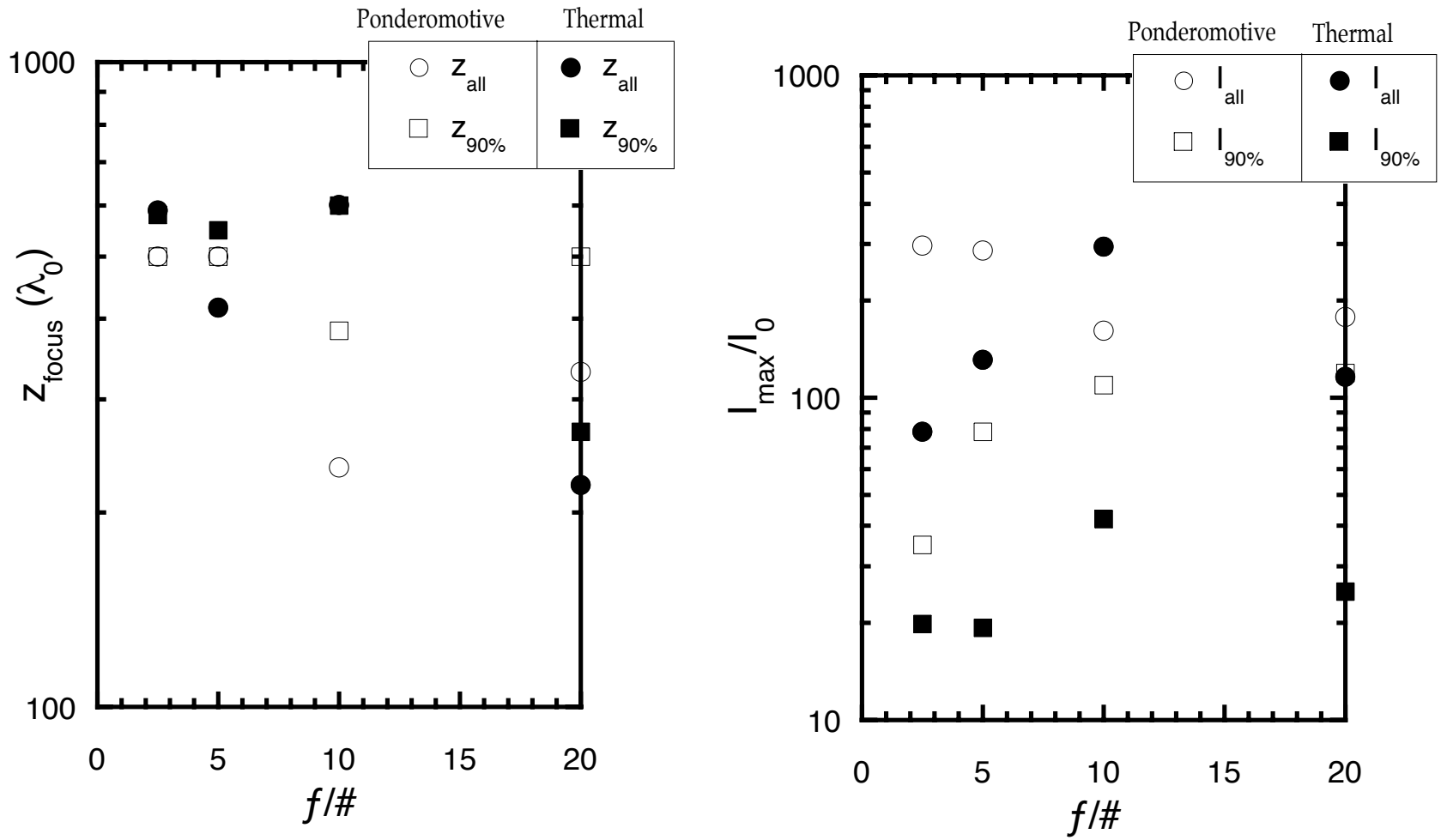
Ponderomotive
Thermal
1000
100
z_{focus} (λ_0)
z_{all}
$z_{90\%}$
0
5
10
15
20
f/#
Ponderomotive
Thermal
1000
100
10
I_{max}/I_0
I_{all}
$I_{90\%}$
0
5
10
15
20
f/#

Fig. 5

(a) Instantaneous intensity profiles

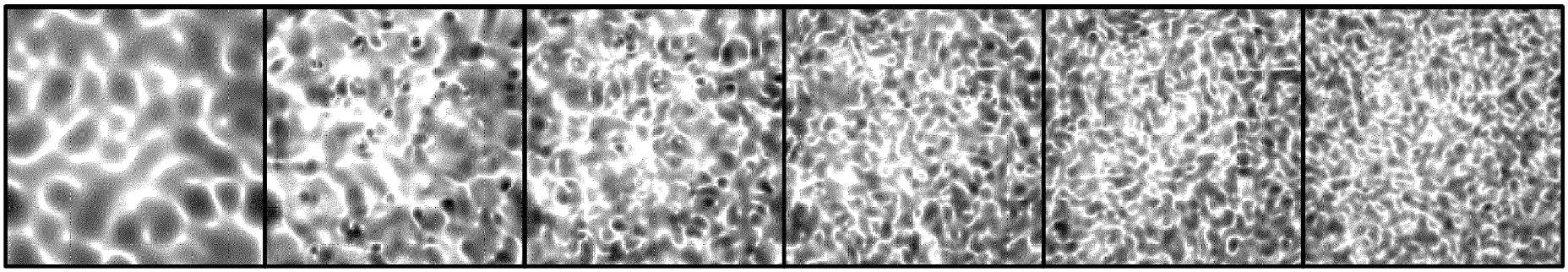

Propagation direction

(b) Time averaged intensity profiles

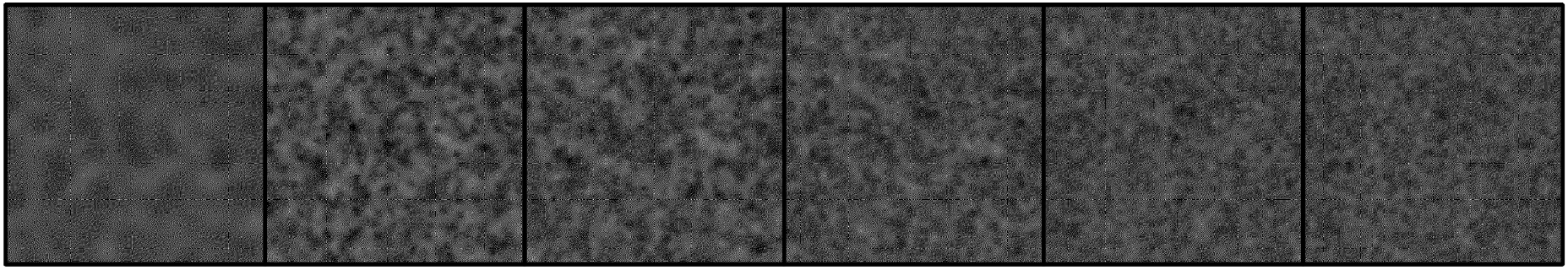

Fig. 6

(a) Instantaneous intensity profiles

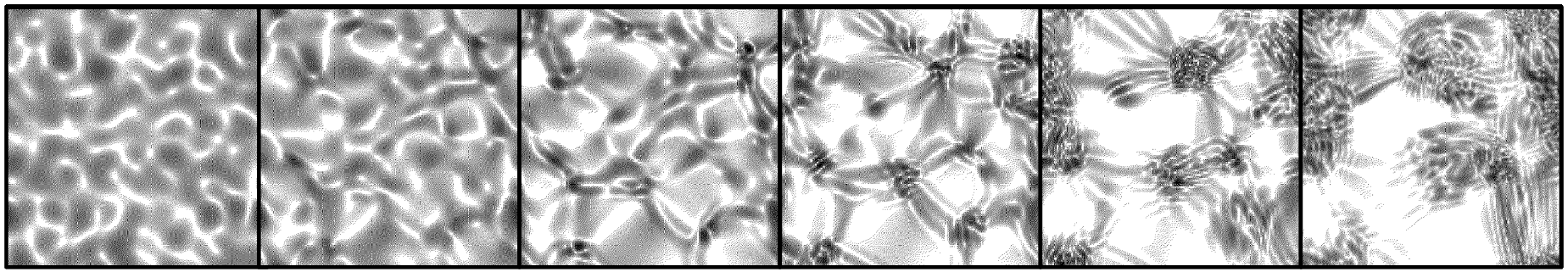

Propagation direction →

(b) Time averaged intensity profiles

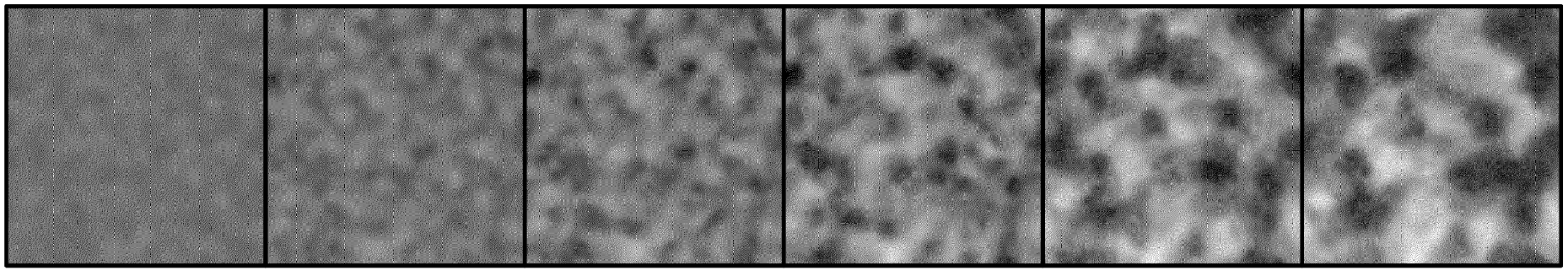

Fig. 7

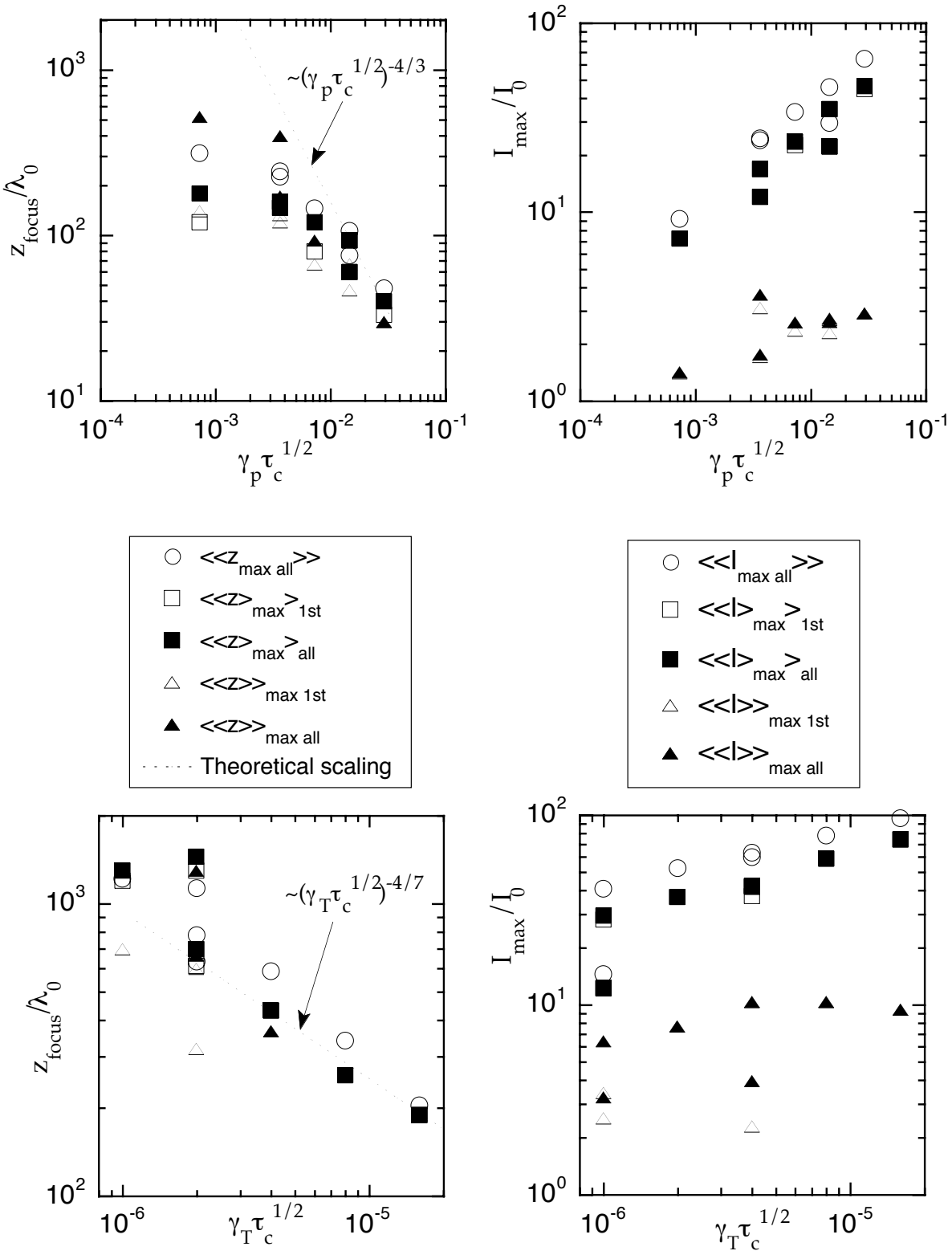
z_{focus}/λ_0
$\sim(\gamma_p\tau_c^{1/2})^{-4/3}$
$\gamma_p\tau_c^{1/2}$
I_{max}/I_0
$\gamma_p\tau_c^{1/2}$
<<z_max all>>
<<z>_max>_1st
<<z>_max>_all
<<z>>_max 1st
<<z>>_max all
Theoretical scaling
<<I_max all>>
<<I>_max>_1st
<<I>_max>_all
<<I>>_max 1st
<<I>>_max all
z_{focus}/λ_0
$\sim(\gamma_T\tau_c^{1/2})^{-4/7}$
$\gamma_T\tau_c^{1/2}$
I_{max}/I_0
$\gamma_T\tau_c^{1/2}$

Fig. 8

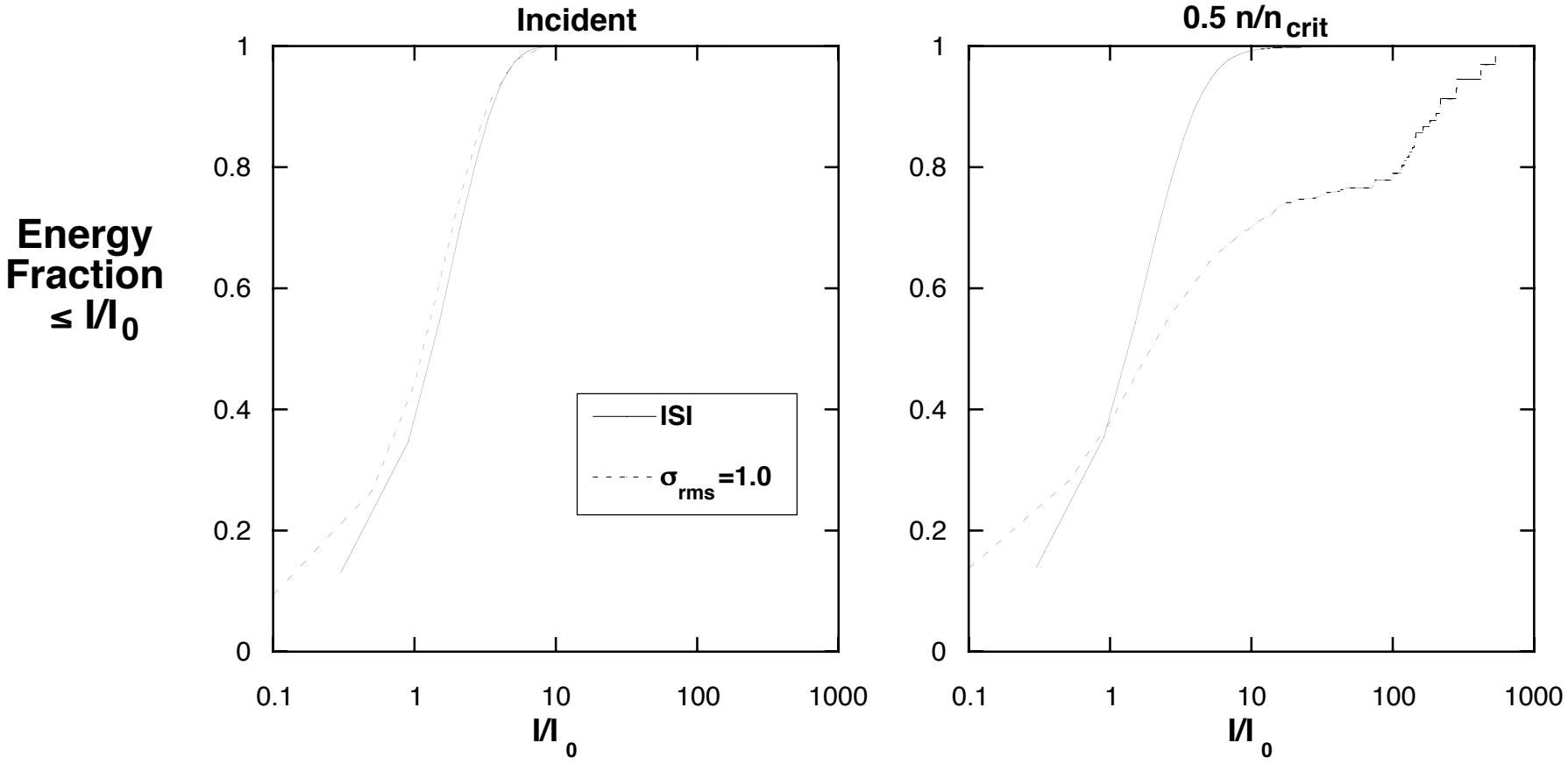
Incident
0.5 n/n crit
Energy Fraction ≤ I/I0
I/I 0
I/I 0
ISI
σrms=1.0
0
0.2
0.4
0.6
0.8
1
0.1
1
10
100
1000

Fig. 9

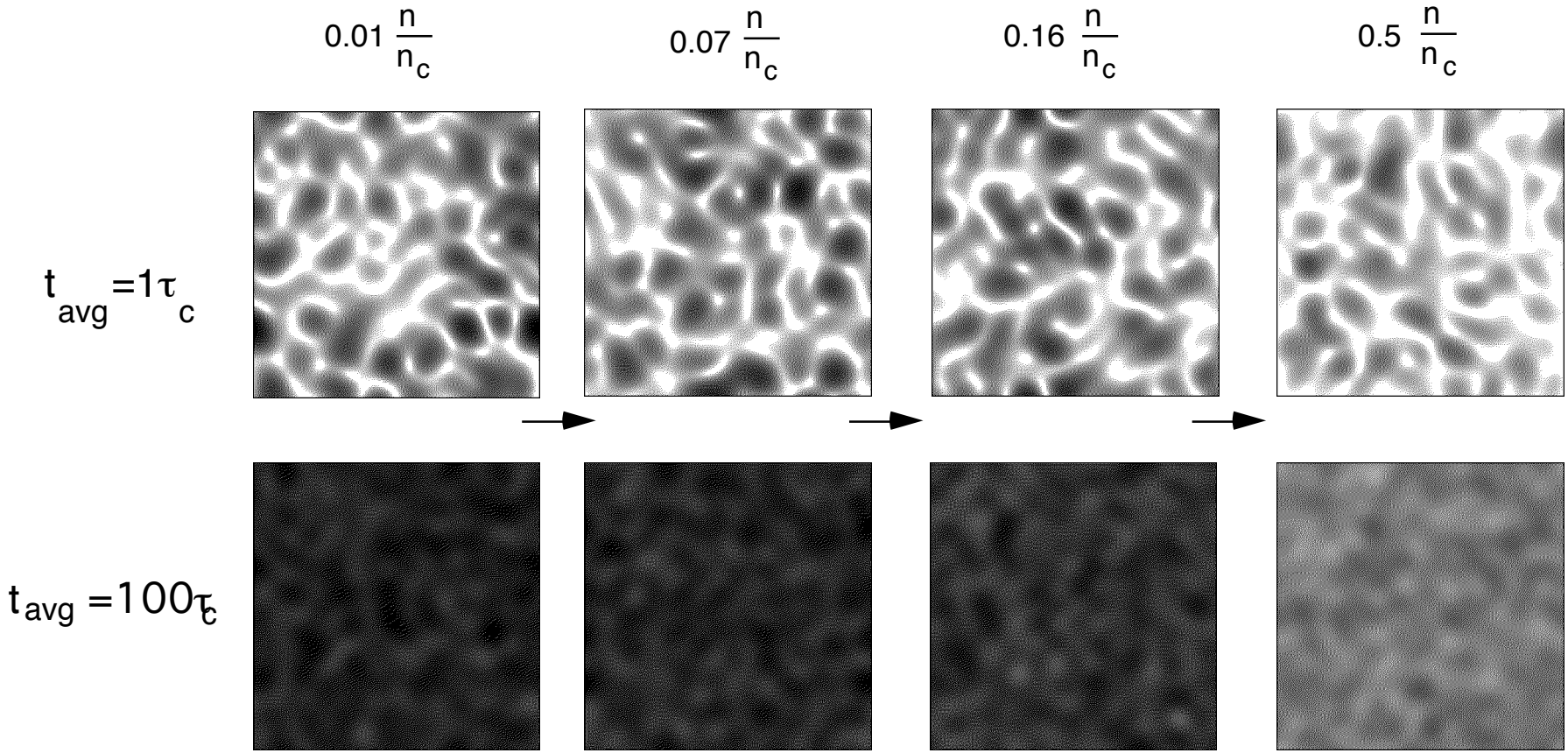

Fig. 10

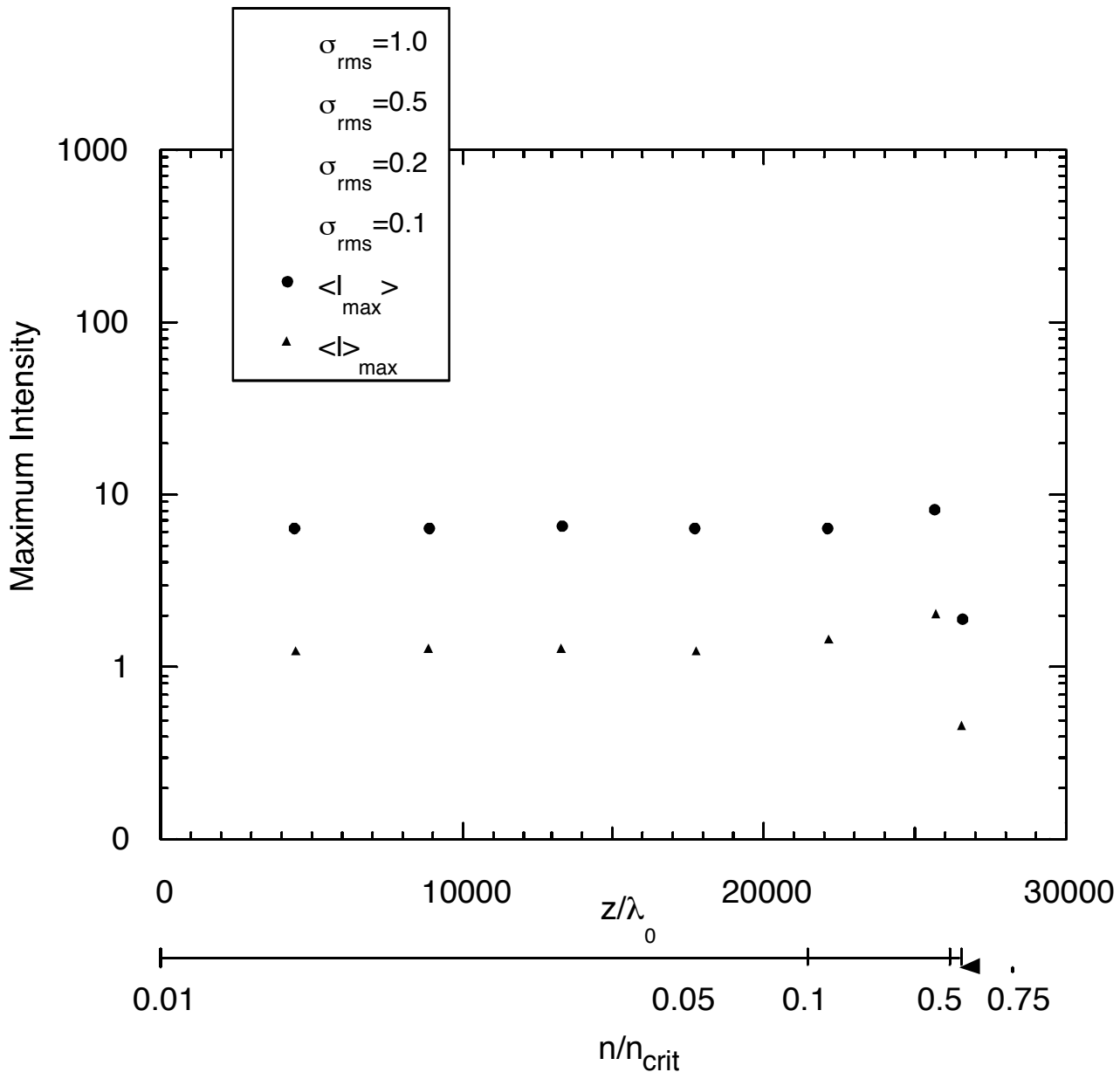
σ rms =1.0
σ rms =0.5
σ rms =0.2
σ rms =0.1
<I max>
<I>max
Maximum Intensity
1000
100
10
1
0
0
10000
20000
30000
z/λ0
0.01
0.05
0.1
0.5
0.75
n/ncrit

Fig. 11